vessels in the diaphragm can be evaluated not only by using tissue sections but also by using whole-mount samples. Using this model, we examined the effects of etodolac on tumor lymphangiogenesis. Etodolac or vehicle control was continuously given for 2 weeks from the time of inoculation of cancer cells to evaluation of lymphangiogenesis. We observed the lymphatic vessels in the diaphragm by whole-mount immunostaining for LYVE-1 from the pleural side. More sprouts were detected along lymphatic vessels over the entire diaphragm in the cancer-inoculated mice than in the cancer-free mice (Fig. 2*B*). However, the number of sprouts was less in the etodolac-treated mice than in the untreated mice (Fig. 2*B*). Quantification of lymphatic sprouts revealed significant reduction of lymphangiogenesis by treatment with etodolac (Fig. 2*C*).

Expression of VEGF-C/VEGF-D and COX-2 in tumor tissues. Macrophages have been suggested to be the major cellular sources of lymphangiogenic growth factors VEGF-C and VEGF-D (10–12). To determine whether macrophages are also the major source of these ligands in our model, we did immunohistochemical staining for macrophage marker F4/80 and VEGF-C or VEGF-D. In this model, many cells positive for VEGF-C (Fig. 3*A*, *a*) and VEGF-D (Fig. 3*A*, *b*) were F4/80-positive macrophages. Although certain cancer cells have also been reported to secrete these ligands, OCUM-2MLN cells were negative for VEGF-C (Fig. 3*A*, *a*) and VEGF-D (Fig. 3*A*, *b*) staining. These observations indicate that macrophages are the major sources of lymphangiogenic growth factors in this model.

We further examined the expression of COX-2 to determine which cells are the targets of the COX-2 inhibitor etodolac. Some lymphatic endothelial cells (Fig. 3*B*) and OCUM-2MLN cells (Fig. 3*C*) expressed COX-2. As shown in Fig. 3*C*, some F4/80-positive macrophages were also COX-2 positive. These findings suggest that etodolac may act on several different types of cells in this model.

We also investigated the expression levels of mouse mRNA for VEGF-C (Fig. 3*D*, *top*) and VEGF-D (Fig. 3*D*, *bottom*) in the tumor tissues. Consistent with the results obtained by immunohistochemical analysis, mRNA level for VEGF-C and VEGF-D increased in the orthotopically inoculated tumors. In addition, the expression of VEGF-C, but not that of VEGF-D, was down-regulated after treatment with etodolac.

Effects of etodolac on macrophages, lymphatic endothelial cells, and cancer cells *in vitro*. Given the coexpression of COX-2 and VEGF-C or VEGF-D in macrophages, we hypothesized that etodolac suppresses the expression of VEGF-C and VEGF-D in macrophages. To test this hypothesis, we examined the mRNA levels of VEGF-C and VEGF-D in *in vitro*–cultured RAW264.7, a mouse macrophage-like cell line, by quantitative RT-PCR. The levels of expression of COX-2 (Fig. 4*A*) and VEGF-C (Fig. 4*B*) were dose-dependently up-regulated at 24 h after stimulation with LPS. The up-regulation of VEGF-C was, however, suppressed by

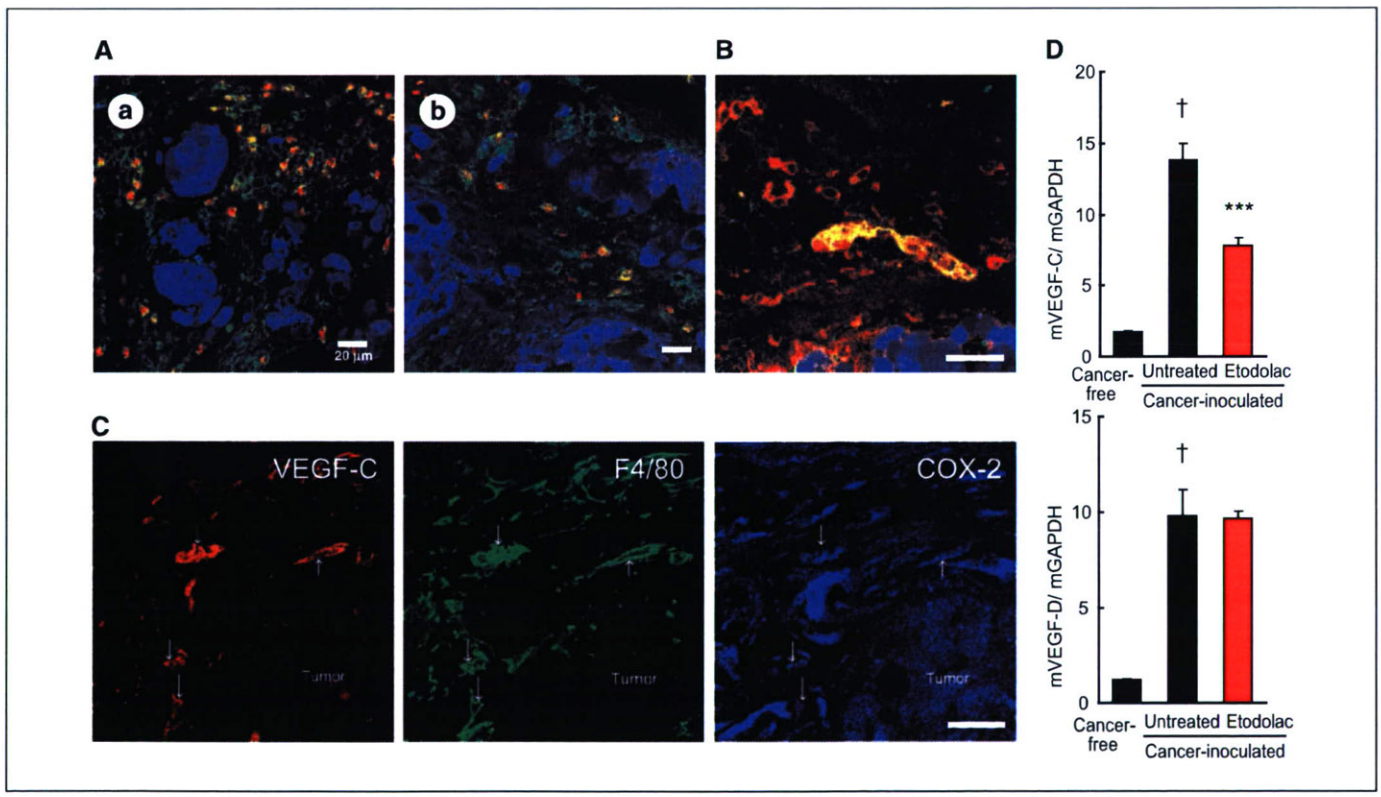

Figure 3. Expression of VEGF-C, VEGF-D, and COX-2 in tumor tissue. *A*, immunostaining of orthotopically inoculated tumors for VEGF-C (*a*) or VEGF-D (*b*, *red*), macrophages (anti-F4/80, *green*), and cancer cells (GFP, *blue*). Note that OCUM-2MLN cells themselves were negative for VEGF-C and VEGF-D. *Scale bar*, 20 μm. *B*, several lymphatic endothelial cells (anti–LYVE-1, *red*) in the GFP-expressing tumor (*blue*) overexpress COX-2 (*green*), suggesting that lymphatic endothelial cells in the tumor are also targets of etodolac. *Scale bar*, 20 μm. *C*, triple immunostaining for VEGF-C, F4/80, and COX-2 in the model of carcinomatous peritonitis showed colocalization of these markers. Most VEGF-C–positive cells were F4/80-positive macrophages, whereas some F4/80-positive macrophages were strongly positive for COX-2. *Arrows*, triple-positive cells. *Scale bar*, 20 μm. *D*, quantitative RT-PCR analysis of mouse mRNA for VEGF-C (*mVEGF-C*, *top*) and mouse mRNA for VEGF-D (*mVEGF-D*) expression (*bottom*). Both mouse mRNA for VEGF-C and VEGF-D increased in orthotopically inoculated tumors, and the expression of mouse mRNA for VEGF-C was down-regulated after 3 d of treatment with etodolac. *Columns*, mean; *bars*, SE. Cancer-inoculated control mice versus cancer-free mice: †, $P < 0.001$; etodolac-treated mice versus cancer-inoculated control mice: ***, $P < 0.001$.

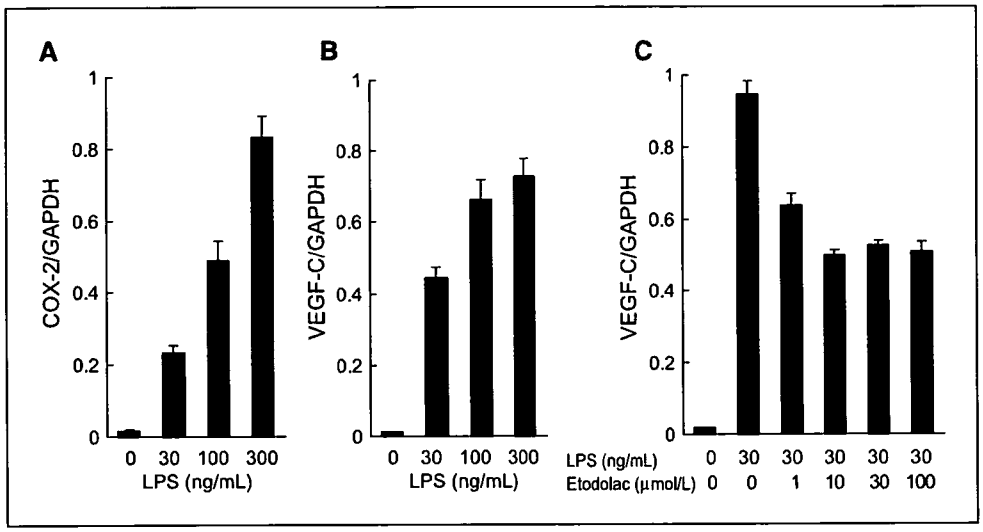

Figure 4. Suppression of expression of VEGF-C by etodolac in macrophages *in vitro*. mRNA levels of COX-2 (*A*) and VEGF-C (*B*) in cultured RAW.264.7, mouse macrophage-like cells, were determined at 24 h after stimulation with LPS. *C*, suppression of VEGF-C expression by treatment with etodolac. *Columns*, mean; *bars*, SE.

treatment with etodolac in a dose-dependent fashion. Ten micromolars or higher concentrations of etodolac maximally, although not completely, suppressed the expression of VEGF-C mRNA (Fig. 4*C*). We also examined the expression of VEGF-D, but found that it was not significantly affected by etodolac (data not shown).

We further examined the effects of etodolac on cells other than macrophages which are involved in tumor lymphangiogenesis, i.e., lymphatic endothelial cells and cancer cells. We used HDLECs to investigate the effects of etodolac on lymphatic endothelial cells. The mRNA levels of VEGF-R3 in HDLECs were not affected by 10 μmol/L of etodolac (Fig. 5*A*). In contrast, cell growth assay revealed that 3 and 30 μmol/L of etodolac each significantly suppressed the growth of HDLECs, only upon stimulation with LPS, although the inhibitory effect of etodolac was not prominent (Fig. 5*B*). We also examined the effects of etodolac on the growth of OCUM-2MLN. However, no significant difference in growth of OCUM-2MLN cells was observed at 3 days after addition of 3 or 30 μmol/L etodolac (Fig. 5*C*).

Suppression of lymphangiogenesis by etodolac in a mouse model of chronic inflammation. We used a mouse model of chronic inflammation to determine whether the suppressive effect of etodolac on tumor lymphangiogenesis holds true for inflammatory lymphangiogenesis. In this model, thioglycollate medium was given i.p. as a proinflammatory agent to induce chronic aseptic peritonitis. After repeated i.p. injection (thrice a week for 2 weeks) of thioglycollate medium to immunocompetent BALB/c mice, inflammatory plaques formed on the peritoneal surface of the diaphragm (Fig. 6*A*, *top*). These plaques were consisted mainly

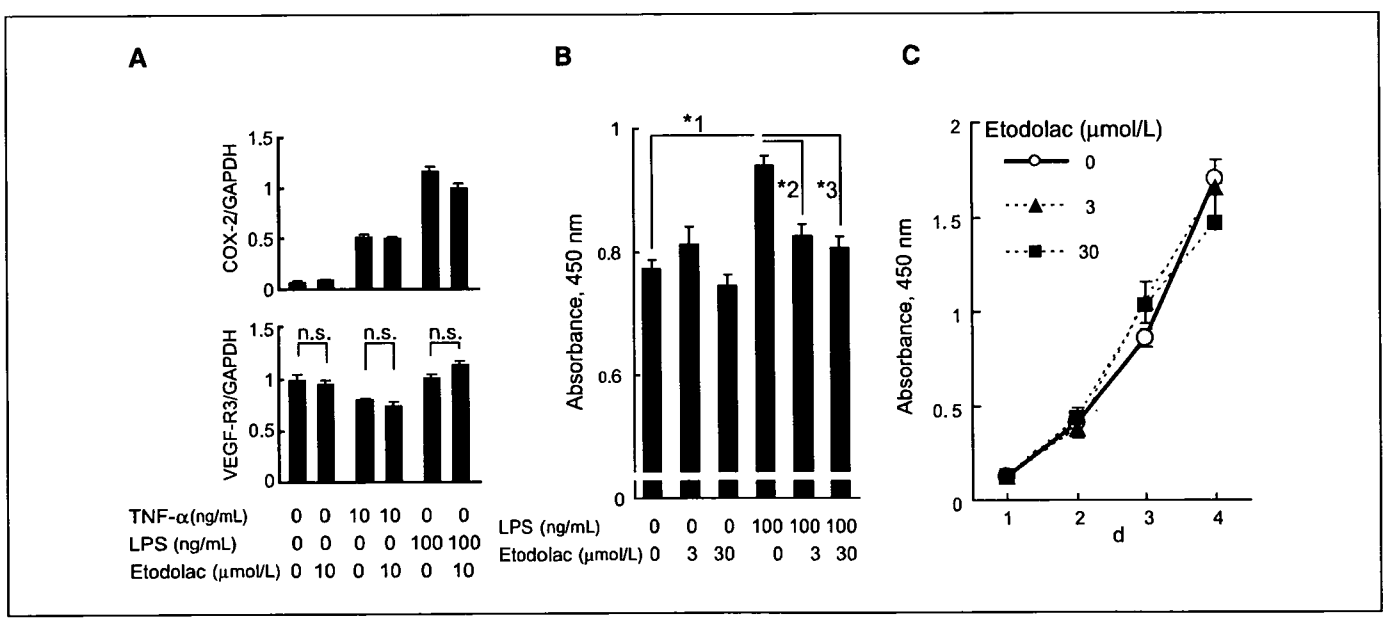

Figure 5. Effects of etodolac on cells other than macrophages. *A*, mRNA levels of VEGF-R3 (*bottom*) in HDLECs treated with 10 μmol/L of etodolac with or without stimulation with 10 ng/mL tumor necrosis factor-α (TNF-α) or 100 ng/mL LPS. *Top*, up-regulation of COX-2 in HDLECs by stimulation with TNF-α or LPS. *Columns*, mean; *bars*, SE. n.s., not significant. *B*, cell growth assay using WST-8 revealed that 3 and 30 μmol/L of etodolac each significantly suppressed the growth of HDLECs upon stimulation with 100 ng/mL LPS; *1, $P < 0.001$; *2, $P < 0.001$; *3, $P < 0.001$; Student's *t* test. *Columns*, mean; *bars*, SE. *C*, cell growth assay with WST-8 revealed that growth of OCUM-2MLN was not affected by etodolac at 3 d after addition of 3 or 30 μmol/L etodolac. *Points*, mean; *bars*, SE.

of mononuclear cells (Fig. 6*A*, *bottom*). Immunohistochemical analysis revealed that COX-2, VEGF-C, and VEGF-D were highly expressed in these plaques and that many cells positive for VEGF-C and VEGF-D were F4/80-positive macrophages (Fig. 6*B*).

Using this model, we examined whether etodolac inhibits inflammatory lymphangiogenesis. As shown in Fig. 6*C*, outgrowths of lymphatic vessels in the plaques were decreased in etodolac-treated mice compared with untreated mice. Quantification of LYVE-1–positive areas in the plaques revealed that induction of lymphangiogenesis was significantly suppressed in etodolac-treated mice compared with control mice (Fig. 6*D*). These findings indicate that etodolac is able to suppress lymphangiogenesis in tumor tissues, as well as in nontumorous tissue.

Discussion

Many clinical and animal studies have shown that COX-2 induces angiogenesis (34). Meanwhile, there is no direct evidence of a relationship between COX-2 and lymphangiogenesis, although some clinical and animal studies have suggested that level of COX-2 expression in tumor tissue is correlated with lymph node metastasis and/or unfavorable prognosis (24–28, 35). However, none of these studies clearly indicated the status of lymphatic vessels. In the present study, we investigated the effects of COX-2 inhibitor on lymphatic vessels using the lymphatic endothelial cell-specific markers LYVE-1 and Prox1. In the model of lymphatic metastasis, both lymphangiogenesis and angiogenesis were induced around the orthotopic tumors of OCUM-2MLN. We found

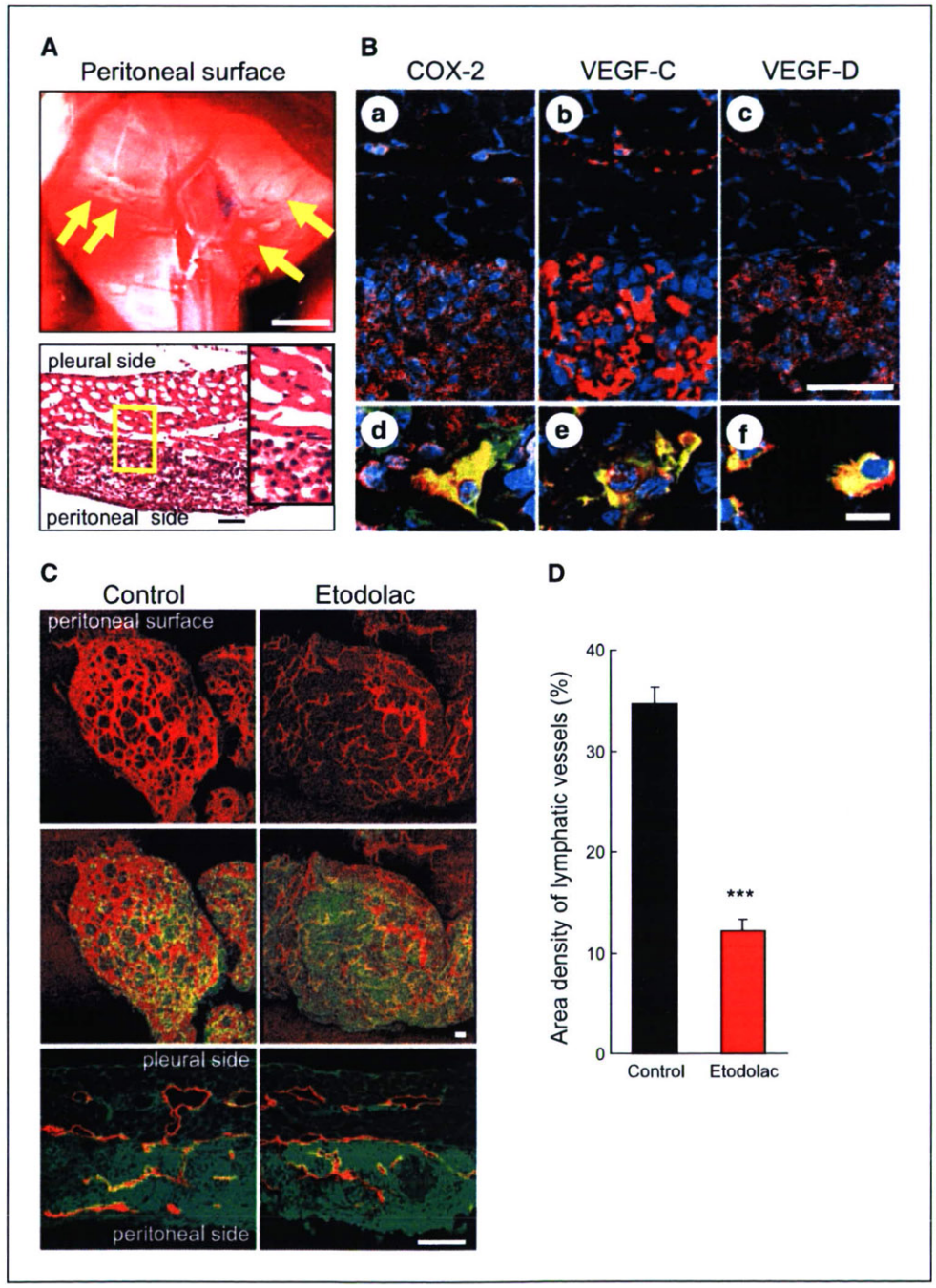

Figure 6. Effects of etodolac on lymphangiogenesis in mouse model of chronic aseptic peritonitis. *A*, *top*, macroscopic appearance of the diaphragm of BALB/c mouse after repeated i.p. injection (thrice a week for 2 wk) of thioglycollate medium. Inflammatory plaques formed on the peritoneal surface of the diaphragm (*arrows*). *Scale bar*, 5 mm. *Bottom*, H&E staining of cross-section of inflammatory plaques on diaphragm. *Scale bar*, 50 μm. *Inset*, enlargement of the boxed area. *B*, immunohistochemical staining of COX-2 (*a and d*), VEGF-C (*b and e*), and VEGF-D (*c and f*) in plaques on diaphragms. Each antibody was displayed in the red channel. *d–f*, double-staining with each antibody and anti-F4/80 (*green*). Nuclear counterstaining was done with TOTO-3 (*blue*). *Scale bars*, 50 μm (*a–c*) and 10 μm (*d–f*). *C*, immunostaining of the inflammatory plaques on diaphragm from control or etodolac-treated mice ($n = 5$ for each group). *Top*, whole-mount staining with the lymphatic vessel marker (anti–LYVE-1, *red*); *middle*, merged images stained also with macrophage marker (anti-CD11b, *green*); *bottom*, cross-sections stained for F4/80 (*green*) and LYVE-1 (*red*). *Scale bar*, 50 μm. *D*, quantification of lymphatic vessels in plaques. *Columns*, mean area densities of LYVE-1–positive pixels per microscopic field; *bars*, SE (10 fields per mouse); ***, $P < 0.001$.

that administration of etodolac suppressed tumor lymphangiogenesis along with tumor angiogenesis. In addition, we evaluated the extent of lymph node metastasis and found that the total weight of metastasized lymph nodes was also decreased by treatment with etodolac. These findings indicated that COX-2 promotes tumor lymphangiogenesis and consequent lymph node metastasis, in addition to tumor angiogenesis as previously reported.

The reproducibility of assignment of highly vascularized areas, i.e., hotspots in tumor tissue sections, is a critical variable in the analysis of lymphangiogenesis (36). Finding relevant hotspots requires training and experience (37). To deal with this potential problem, we established here a new model of tumor lymphangiogenesis in the diaphragm. Since lymphatic vessels in the diaphragm can be immunostained in whole-mount preparations, it is possible to capture the entire network of lymphatics in the diaphragm. There is no need to pick only hotspots for quantification because outgrowth of lymphatic vessels was observed over the entire diaphragm in the model of carcinomatous peritonitis. We quantified the number of sprouts of lymphatic vessels as a marker of lymphangiogenesis, as suggested by Baluk et al. (11). The results using this model confirmed the finding that etodolac suppresses lymphangiogenesis.

Recent studies have shown that inflammatory cells have stimulatory effects on tumor progression (38). In particular, tumor-associated macrophages have been suggested to promote tumor lymphangiogenesis (10, 39). We therefore hypothesized that etodolac suppresses the secretion of lymphangiogenic factors from macrophages. Our finding that some macrophages in tumor stroma expressed COX-2 strongly supports this hypothesis. Furthermore, we found that mRNA levels of VEGF-C was indeed suppressed by etodolac in RAW264.7 cells, as well as in tumor tissues *in vivo*. Although these findings are not in agreement with a previous report that VEGF-C expression in fibroblasts was not suppressed by indomethacin, a nonselective NSAID (40), this discrepancy may be due to the difference in cell types examined or the COX-2 selectivity of drugs used.

Lymphangiogenesis is also induced in chronic inflammatory lesions (41). Macrophages have recently been shown to be recruited into inflammatory lesions to secrete VEGF-C and induce lymphangiogenesis (11, 12). In the present study, using a model of chronic aseptic peritonitis, we observed that macrophages densely accumulated in inflammatory plaques, wherein lymphangiogenic growth factors are expressed. These findings suggest that COX-2 can enhance lymphangiogenesis in the absence of cancer cells.

We have shown that decrease of lymph node metastasis can be achieved by COX-2 inhibitor, possibly via inhibition of macrophage-mediated lymphangiogenesis. Despite recent studies reporting cardiovascular complications from long-term administration of NSAIDs (42), these drugs may still be applicable to cancer treatment by limiting population and administrating periods: NSAIDs should be effective for preventing potential metastases in patients with advanced cancers in presurgical period or in those having inflammation aroused by surgical manipulation in early postsurgical periods. In the latter case, surgery-related inflammation may be accompanied by lymphangiogenesis, which can be a cause of dissemination or metastasis of unexpectedly remained cancer cells.

In conclusion, we believe that our findings may provide a potential usage of COX-2 inhibitors in cancer treatment, which could overcome known obstacles in using these drugs.

Acknowledgments

Received 6/26/2007; revised 8/27/2007; accepted 9/5/2007.

Grant support: KAKENHI, a grant-in-aid for scientific research from the Ministry of Education, Culture, Sports, Science, and Technology of Japan.

The costs of publication of this article were defrayed in part by the payment of page charges. This article must therefore be hereby marked *advertisement* in accordance with 18 U.S.C. Section 1734 solely to indicate this fact.

We thank Arisa Mita for expert technical assistance.

References

1. Alitalo K, Tammela T, Petrova TV. Lymphangiogenesis in development and human disease. Nature 2005;438:946–53.
2. Achen MG, Stacker SA. Tumor lymphangiogenesis and metastatic spread-new players begin to emerge. Int J Cancer 2006;119:1755–60.
3. Pepper MS. Lymphangiogenesis and tumor metastasis: myth or reality? Clin Cancer Res 2001;7:462–8.
4. Pepper MS, Tille JC, Nisato R, Skobe M. Lymphangiogenesis and tumor metastasis. Cell Tissue Res 2003;314:167–77.
5. Nakamura Y, Yasuoka H, Tsujimoto M, et al. Importance of lymph vessels in gastric cancer: a prognostic indicator in general and a predictor for lymph node metastasis in early stage cancer. J Clin Pathol 2006;59:77–82.
6. Achen MG, McColl BK, Stacker SA. Focus on lymphangiogenesis in tumor metastasis. Cancer Cell 2005;7:121–7.
7. Shimizu K, Kubo H, Yamaguchi K, et al. Suppression of VEGFR-3 signaling inhibits lymph node metastasis in gastric cancer. Cancer Sci 2004;95:328–33.
8. Yonemura Y, Endo Y, Fujita H, et al. Role of vascular endothelial growth factor C expression in the development of lymph node metastasis in gastric cancer. Clin Cancer Res 1999;5:1823–9.
9. Kitadai Y, Kodama M, Cho S, et al. Quantitative analysis of lymphangiogenic markers for predicting metastasis of human gastric carcinoma to lymph nodes. Int J Cancer 2005;115:388–92.
10. Schoppmann SF, Birner P, Stockl J, et al. Tumor-associated macrophages express lymphatic endothelial growth factors and are related to peritumoral lymphangiogenesis. Am J Pathol 2002;161:947–56.
11. Baluk P, Tammela T, Ator E, et al. Pathogenesis of persistent lymphatic vessel hyperplasia in chronic airway inflammation. J Clin Invest 2005;115:247–57.
12. Cursiefen C, Chen L, Borges LP, et al. VEGF-A stimulates lymphangiogenesis and hemangiogenesis in inflammatory neovascularization via macrophage recruitment. J Clin Invest 2004;113:1040–50.
13. Thun MJ, Henley SJ, Patrono C. Nonsteroidal anti-inflammatory drugs as anticancer agents: mechanistic, pharmacologic, and clinical issues. J Natl Cancer Inst 2002;94:252–66.
14. Dannenberg AJ, Altorki NK, Boyle JO, et al. Cyclooxygenase 2: a pharmacological target for the prevention of cancer. Lancet Oncol 2001;2:544–51.
15. Ristimaki A, Honkanen N, Jankala H, Sipponen P, Harkonen M. Expression of cyclooxygenase-2 in human gastric carcinoma. Cancer Res 1997;57:1276–80.
16. Saukkonen K, Nieminen O, van Rees B, et al. Expression of cyclooxygenase-2 in dysplasia of the stomach and in intestinal-type gastric adenocarcinoma. Clin Cancer Res 2001;7:1923–31.
17. Oshima M, Dinchuk JE, Kargman SL, et al. Suppression of intestinal polyposis in $Apc^{\Delta 716}$ knockout mice by inhibition of cyclooxygenase 2 (COX-2). Cell 1996;87:803–9.
18. Kawamori T, Rao CV, Seibert K, Reddy BS. Chemopreventive activity of celecoxib, a specific cyclooxygenase-2 inhibitor, against colon carcinogenesis. Cancer Res 1998;58:409–12.
19. Wang D, Mann JR, DuBois RN. The role of prostaglandins and other eicosanoids in the gastrointestinal tract. Gastroenterology 2005;128:1445–61.
20. Tsujii M, Kawano S, Tsuji S, Sawaoka H, Hori M, DuBois RN. Cyclooxygenase regulates angiogenesis induced by colon cancer cells. Cell 1998;93:705–16.
21. Williams CS, Tsujii M, Reese J, Dey SK, DuBois RN. Host cyclooxygenase-2 modulates carcinoma growth. J Clin Invest 2000;105:1589–94.
22. Leahy KM, Ornberg RL, Wang Y, Zweifel BS, Koki AT, Masferrer JL. Cyclooxygenase-2 inhibition by celecoxib reduces proliferation and induces apoptosis in angiogenic endothelial cells *in vivo*. Cancer Res 2002;62:625–31.
23. Masferrer JL, Leahy KM, Koki AT, et al. Antiangiogenic and antitumor activities of cyclooxygenase-2 inhibitors. Cancer Res 2000;60:1306–11.
24. Su JL, Shih JY, Yen ML, et al. Cyclooxygenase-2 induces EP1- and HER-2/Neu-dependent vascular endothelial growth factor-C up-regulation: a novel mechanism of lymphangiogenesis in lung adenocarcinoma. Cancer Res 2004;64:554–64.
25. Timoshenko AV, Chakraborty C, Wagner GF, Lala PK. COX-2-mediated stimulation of the lymphangiogenic factor VEGF-C in human breast cancer. Br J Cancer 2006;94:1154–63.
26. Siironen P, Ristimaki A, Narko K, et al. VEGF-C and

COX-2 expression in papillary thyroid cancer. Endocr Relat Cancer 2006;13:465–73.
27. Soumaoro LT, Uetake H, Takagi Y, et al. Coexpression of VEGF-C and Cox-2 in human colorectal cancer and its association with lymph node metastasis. Dis Colon Rectum 2006;49:392–8.
28. Zhang J, Ji J, Yuan F, et al. Cyclooxygenase-2 expression is associated with VEGF-C and lymph node metastases in gastric cancer patients. Biomed Pharmacother 2005;59 [Suppl]:S285–8.
29. Glaser K, Sung ML, O'Neill K, et al. Etodolac selectively inhibits human prostaglandin G/H synthase 2 (PGHS-2) versus human PGHS-1. Eur J Pharmacol 1995;281:107–11.
30. Warner TD, Giuliano F, Vojnovic I, Bukasa A, Mitchell JA, Vane JR. Nonsteroid drug selectivities for cyclo-oxygenase-1 rather than cyclo-oxygenase-2 are associated with human gastrointestinal toxicity: a full *in vitro* analysis. Proc Natl Acad Sci U S A 1999;96:7563–8.
31. Fujihara T, Sawada T, Hirakawa K, et al. Establishment of lymph node metastatic model for human gastric cancer in nude mice and analysis of factors associated with metastasis. Clin Exp Metastasis 1998;16:389–98.
32. Shibuya K, Shirakawa J, Kameyama T, et al. CD226 (DNAM-1) is involved in lymphocyte function-associated antigen 1 costimulatory signal for naive T cell differentiation and proliferation. J Exp Med 2003;198:1829–39.
33. Abu-Hijleh MF, Habbal OA, Moqattash ST. The role of the diaphragm in lymphatic absorption from the peritoneal cavity. J Anat 1995;186:453–67.
34. Iniguez MA, Rodriguez A, Volpert OV, Fresno M, Redondo JM. Cyclooxygenase-2: a therapeutic target in angiogenesis. Trends Mol Med 2003;9:73–8.
35. Tendo M, Yashiro M, Nakazawa K, et al. Inhibitory effect of a selective cyclooxygenase inhibitor on the invasion-stimulating activity of orthotopic fibroblasts for scirrhous gastric cancer cells. Cancer Sci 2005;96:451–5.
36. Van der Auwera I, Cao Y, Tille JC, et al. First international consensus on the methodology of lymphangiogenesis quantification in solid human tumours. Br J Cancer 2006;95:1611–25.
37. Vermeulen PB, Gasparini G, Fox SB, et al. Second international consensus on the methodology and criteria of evaluation of angiogenesis quantification in solid human tumours. Eur J Cancer 2002;38:1564–79.
38. Coussens LM, Werb Z. Inflammation and cancer. Nature 2002;420:860–7.
39. Dadras SS, Paul T, Bertoncini J, et al. Tumor lymphangiogenesis: a novel prognostic indicator for cutaneous melanoma metastasis and survival. Am J Pathol 2003;162:1951–60.
40. Ristimaki A, Narko K, Enholm B, Joukov V, Alitalo K. Proinflammatory cytokines regulate expression of the lymphatic endothelial mitogen vascular endothelial growth factor-C. J Biol Chem 1998;273:8413–8.
41. Pullinger BD, Florey HW. Proliferation of lymphatics in inflammation. J Pathol Bact 1937;45:157–70.
42. Antman EM, Bennett JS, Daugherty A, Furberg C, Roberts H, Taubert KA. Use of nonsteroidal antiinflammatory drugs: an update for clinicians: a scientific statement from the American Heart Association. Circulation 2007;115:1634–42.

Available online at www.sciencedirect.com
ScienceDirect
Journal of Controlled Release 121 (2007) 146–155
journal of controlled release
www.elsevier.com/locate/jconrel

Optimization of (1,2-diamino-cyclohexane)platinum(II)-loaded polymeric micelles directed to improved tumor targeting and enhanced antitumor activity

Horacio Cabral [a], Nobuhiro Nishiyama [b], Kazunori Kataoka [a,b,c,*]

[a] *Department of Materials Engineering, Graduate School of Engineering, The University of Tokyo, 7-3-1 Hongo, Bunkyo-ku, Tokyo 113-8656, Japan*
[b] *Center for Disease Biology and Integrative Medicine, Graduate School of Medicine, The University of Tokyo, 7-3-1 Hongo, Bunkyo-ku, Tokyo 113-0033, Japan*
[c] *Center for NanoBio Integration, The University of Tokyo, 7-3-1 Hongo, Bunkyo-ku, Tokyo, 113-8656, Japan*

Received 19 March 2007; accepted 21 May 2007
Available online 29 May 2007

Abstract

Polymeric micelles are promising nanocarriers, which might enhance the efficacy of antitumor drugs. Herein, polymeric micelles incorporating dichloro(1,2-diamino-cyclohexane)platinum(II) (DACHPt), the oxaliplatin parent complex, were prepared through the polymer-metal complex formation of DACHPt with poly(ethylene glycol)-*b*-poly(glutamic acid) [PEG-*b*-P(Glu)] block copolymer having different lengths of the poly (glutamic acid) block [p(Glu): 20, 40, and 70 U]. The resulting micelles were studied with the aim of optimizing the system's biological performance. DACHPt-loaded micelles (DACHPt/m) were approximately 40 nm in diameter and had a narrow size distribution. *In vivo* biodistribution and antitumor activity experiments (CDF_1 mice bearing the murine colon adenocarcinoma C-26 inoculated subcutaneously) showed 20-fold greater accumulation of DACHPt/m at the tumor site than free oxaliplatin to achieve substantially higher antitumor efficacy. Moreover, the micelles prepared from PEG-*b*-P(Glu) with 20 U of P(Glu) exhibited the lowest non-specific accumulation in the liver and spleen to critically reduce non-specific accumulation, resulting in higher specificity to solid tumors. The antitumor effect of DACHPt/m was also evaluated on multiple metastases generated from intraperitoneally injected bioluminescent HeLa (HeLa-Luc) cells. The *in vivo* bioluminescent data indicated that DACHPt/m decreased the signal 10-to 50-fold compared to the control indicating a very strong antitumor activity. These results suggest that DACHPt/m could be an outstanding drug delivery system for oxaliplatin in the treatment of solid tumors.

Keywords: Polymeric micelles; DACHPt; Oxaliplatin; Biodistribution; Antitumor activity

1. Introduction

Oxaliplatin, oxalato(trans-*l*-1,2-diaminocyclohexane)platinum(II), is a third-generation platinum drug approved by the United States Food and Drug Administration in 2004 for the first-line treatment of advanced colorectal cancer in combination with 5-fluorouracil/folinic acid (5-FU/LV) [1]. The incorporation of oxaliplatin into the colorectal cancer program represents a major improvement in the treatment of the disease. The synergistic effects between oxaliplatin and 5-FU/LV significantly increased the response rates, improved the time-sensitive response parameters, and contributed to the removal of heretofore unresectable hepatic metastases, thereby changing the natural history of the malignancy. Nevertheless, oxaliplatin distributes rapidly to the whole body and, even though it shows better tolerability relative to other platinum drugs, cumulative peripheral distal neurotoxicity and acute dysesthesias restrain the range of working doses [2,3]. Consequently, enormous effort has been dedicated to develop drug delivery systems that increase the blood residence time of oxaliplatin and other platinum drugs, and target those drugs to solid tumors by taking advantage of the enhanced permeability and retention (EPR) effect [4]. Liposomes and macromolecular carriers (water soluble polymer–drug conjugates) have been the first attempts

* Corresponding author. Department of Materials Engineering, Graduate School of Engineering, The University of Tokyo, 7-3-1 Hongo, Bunkyo-ku, Tokyo 113-8656, Japan. Tel.: +81 3 5841 7138; fax: +81 3 5841 7139.
E-mail address: kataoka@bmw.t.u-tokyo.ac.jp (K. Kataoka).

0168-3659/$ - see front matter © 2007 Elsevier B.V. All rights reserved.
doi:10.1016/j.jconrel.2007.05.024

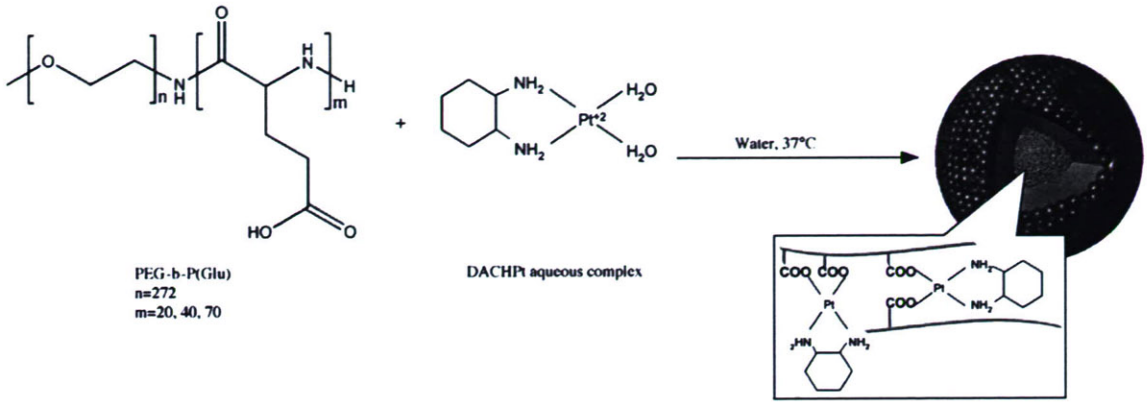

Fig. 1. Formation of DACHPt-loaded micelle (DACHPt/m).

to be considered [5–11]. However, successful formulations have not been developed yet due to unfavorable properties of platinum drugs. For example, the low water solubility of platinum drugs limits their loading efficacy into liposomal formulations (only 1 to 7% of drug loading). Moreover, liposomes incorporating the drug in the lipid bilayer showed rapid leakage of the drugs during storage and in the bloodstream [6]. In the case of macromolecular-drug formulations at high substitution ratios, they show reduced solubility due to the enlarged cohesive forces and to the cross-linking formation between polymer chains [8].

A novel approach to the design of nanocarriers for platinum drugs has been utilizing polymeric micelles [12–15]. Polymeric micelles present unique advantages over other types of drug-carrier systems: (i) prolonged blood circulation due to the efficient stealthy behavior of the dense shell of poly(ethylene glycol) (PEG), which hinders the adsorption of plasma proteins on the surface of the nanostructure and avoids recognition by the reticuloendothelial system (RES); (ii) easiness in encapsulating different compounds by modulating the micelle-forming block copolymers; (iii) reduced cumulative toxicity because of the micellar self-dissociation into unimers with molecular weight lower than that of the threshold of glomerular excretion; (iv) simplicity in size control by changing the chemical composition of block copolymers; (v) deeper tumor penetration due to the sub-100 nm size; (vi) facile management of the drug release in a controlled and environment-sensitive manner by modification of the drug-polymer system; and (vii) improved targeting capability by conjugating pilot molecules on the surface of micelles.

The first generation of platinum-drug-loaded micelles was prepared by the metal-complex formation between cis-dichlorodiammineplatinum(II) (cisplatin, CDDP) and poly(ethylene glycol)-*b*-poly(amino acid) block copolymers [16–21]. The exceptional physicochemical and biological properties of the CDDP-loaded micelle indicate them as an outstanding delivery system for CDDP complexes and a phase I clinical trial is being performed in United Kingdom (NC-6004, Nanocarrier, Japan). More recently, new platinum-drug-loaded polymeric micelles incorporating the oxaliplatin active complex were prepared by the complexation of dichloro(1,2-diaminocyclohexane)platinum(II) (DACHPt) with PEG-*b*-P(Glu) [22]. Previous studies demonstrated that the DACHPt-loaded micelle (DACHPt/m) might maintain its micellar structure for approximately 10 days in 10 mM PBS plus 150 mM NaCl, considerably longer than the stability of the CDDP-loaded micelles (ca 50 h) under the same conditions, while the drug was released from the micelle core in a sustained manner. Moreover, DACHPt/m showed remarkably prolonged blood circulation and more than 20-fold greater accumulation in tumor tissue compared to free oxaliplatin. According to these results, DACHPt/m seems to be an exceptionally promising carrier for the active complexes of oxaliplatin.

Herein, the *in vitro* and *in vivo* biological properties of DACHPt/m prepared with poly(ethylene glycol)-*b*-poly(glutamic acid) [PEG-*b*-P(Glu)] were studied with the aim of optimizing the biological performance of the micelle. Thus, PEG-*b*-P(Glu) having different P(Glu) block lengths (20, 40, and 70 U) were synthesized and used for the micelle preparation. DACHPt/m was phisicochemically characterized to determine the size, size distribution, zeta-potential, drug loading, and weight fraction of block copolymer. The *in vivo* behavior of DACHPt/m was assessed by the biodistribution and antitumor activity experiments using CDF_1 mice bearing the murine colon adenocarcinoma 26 (C-26). Although oxaliplatin had shown low efficacy against this tumor model [23], we found that DACHPt/m considerably increased the antitumor activity of the drug, probably by maintaining high drug levels within the tumor for a prolonged period. Furthermore, since chemotherapy is used in patients with metastatic disease and all the established therapies reveal poor efficiency at the late stage of the disease [24], new therapeutic strategies are urgently needed. Moreover, given that the very low prognosis of late-stage cervical carcinoma [25] (5 years after treatment 15% or fewer of women with stage IV cancer survive) is mainly due to metastasis to the abdomen or the lungs, the antitumor activity of DACHPt/m was evaluated against a bioluminescent intraperitoneal metastatic tumor model of cervical cancer.

2. Experimental

2.1. Materials

γ-benzyl L-glutamate was purchased from Sigma Chemical (St. Louis, MO). Bis(trichloromethyl)carbonate (triphosgene) was purchased from Tokyo Kasei Kogyo (Tokyo, Japan). *N*,*N*-

Table 1
DACHPt-loaded micelles (DACHPt/m) size, zeta-potential and drug loading

Micelle formulation	Size(nm)	Zeta-potential(mV)	Drug loading, [DACHPt]/[Glu]
DACHPt/m 12–20	37	−3	0.317
DACHPt/m 12–40	40	−4	0.323
DACHPt/m 12–70	41	−4	0.288

Table 2
Accumulation ratios and area under the curve (AUC) ratios between tumor and normal organs at 48 h after administration of DACHPt-loaded micelles (DACHPt/m)[a] prepared with PEG-*b*-P(Glu) 12–40 and free oxaliplatin

Drug	Accumulation ratio				AUC ratio[b]	
	Tumor/ liver	Tumor/ spleen	Tumor/ kidney	Tumor/ liver	Tumor/ spleen	Tumor/ kidney
DACHPt/m 12–40	1.25	1.26	3.9	1.25	1.53	3.12
Oxaliplatin	0.9	0.18	0.42	1.1	0.32	0.9

[a] Dose: 0.1 mg per mouse on Pt basis.
[b] AUC calculated by trapezoidal rule up to 48 h.

dimethylformamide (DMF) and 3-(4,5-dimethylthiazol-2-yl)-2,5-diphenyltetrazolium bromide (MTT) were obtained from Wako Pure Chemical (Osaka, Japan). Dichloro(1,2-diammino-cyclohexane)platinum(II) (DACHPt) and $AgNO_3$ were purchased from Aldrich Chemical (Milwaukee, WI). α-methoxy-ω-aminopoly(ethylene glycol) (CH_3O–PEG–NH_2; Mw= 12,000) was purchased from Nippon Oil and Fats (Tokyo, Japan).

2.2. Cell lines and animals

Murine colon adenocarcinoma 26 (C-26) cells were kindly supplied by the National Cancer Center (Tokyo, Japan). C-26 cells were maintained in RPMI 1640 medium (Sigma Chemical) containing 10% fetal bovine serum in a humidified atmosphere containing 5% CO_2 at 37 °C. Bioluminescent HeLa (HeLa-Luc) cells were purchased from Xenogen (Alameda, CA). Luciferase stable-HeLa-Luc cells were maintained in Dulbecco's Modified Eagle Medium (Sigma Chemical Co., Inc.) containing 10% fetal bovine serum in a humidified atmosphere containing 5% CO_2 at 37 °C for no more than two weeks to assure luciferase luminescence stability.

Severe Combined Immunodeficiency (SCID) and CDF_1 mice (female; 18–20 g body weight; 6 weeks old) were purchased from Charles River Japan (Kanagawa, Japan). All animal experiments were carried out in accordance with the Guide for the Care and Use of Laboratory Animals as stated by the NIH. Sterile procedures were followed to assure that SCID mice were disease-free.

2.3. Preparation of PEG-b-P(Glu)

PEG-*b*-P(Glu) block copolymers were synthesized in accordance with the previously described synthetic method

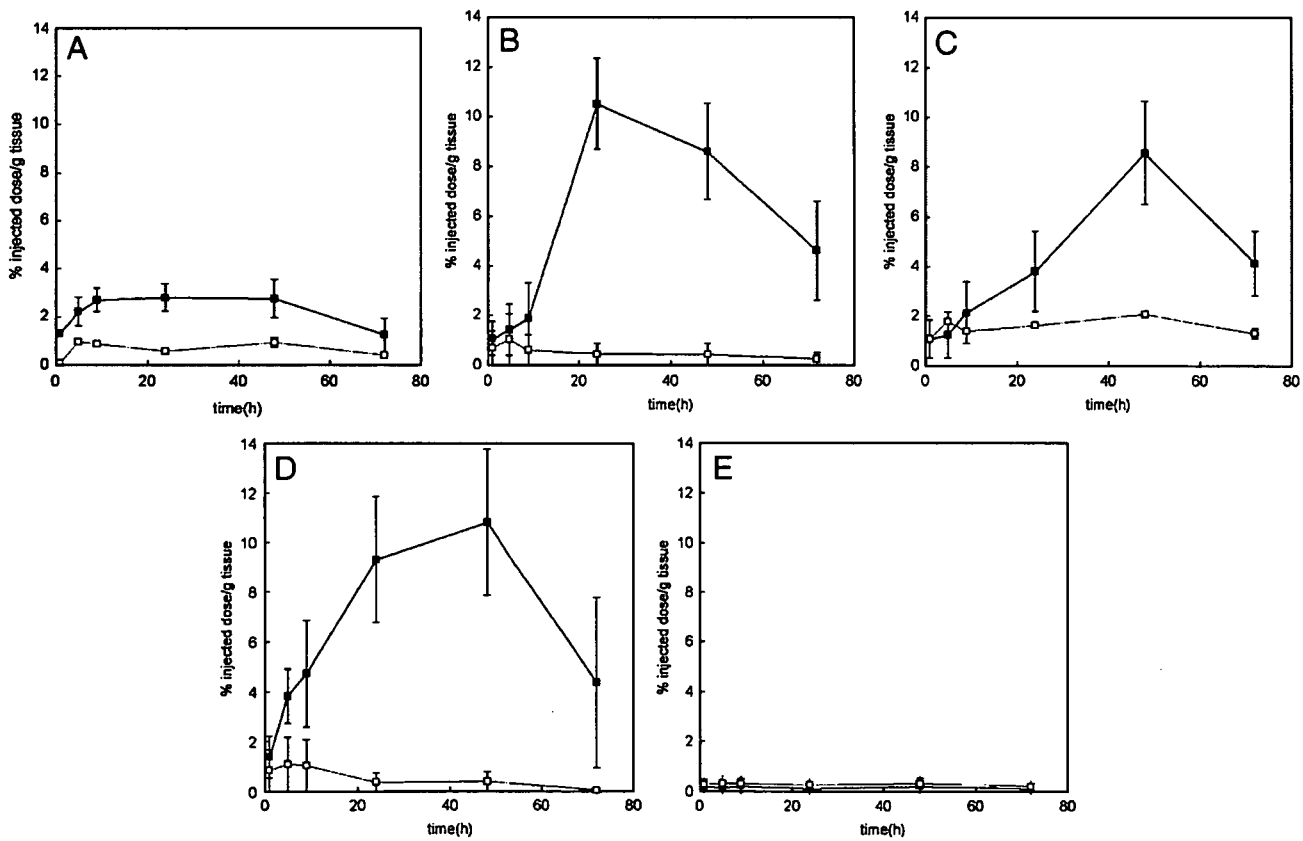

Fig. 2. Biodistribution of oxaliplatin (□) and DACHPt-loaded micelle (DACHPt/m) prepared with PEG-*b*-P(Glu) 12–40 (■): A. Kidney; B. Liver; C. Spleen; D. Tumor; E. Muscle. Data are expressed as averages±S.D.

[20] with a minor modification. Briefly, the *N*-carboxy anhydride of γ-benzyl L-glutamate was synthesized by the Fuchs–Farthing method using triphosgene. Then, *N*-carboxy anhydride of γ-benzyl L-glutamate was polymerized in DMF, initiated by the primary amino group of CH_3O–PEG–NH_2, to obtain PEG-*b*-poly(γ-benzyl L-glutamate) (PEG-*b*-PBLG) block copolymer with different PBLG block lengths (20, 40, and 70 U). The molecular weight distribution of PEG-*b*-PBLG was determined by gel permeation chromatography [column: TSK-gel $G3000_{HHR}$, $G4000_{HHR}$ (Tosoh, Yamaguchi, Japan); eluent: DMF containing 10 mM LiCl; flow rate: 0.8 ml/min; detector: refractive index (RI); temperature: 25 °C]. The polymerization degree of PBLG was verified by comparing the proton ratios of methylene units in PEG ($-OCH_2CH_2-$: δ=3.7 ppm) and phenyl groups of PBLG ($-CH_2C_6H_5$: δ=7.3 ppm) in ^{1}H-NMR measurement [JEOL EX270 (JEOL, Tokyo, Japan); solvent: DMSO-d_6; temperature: 80 °C]. PEG-*b*-PBLG was deprotected by mixing with 0.5 N NaOH at room temperature to obtain PEG-*b*-P(Glu). Complete deprotection was confirmed by ^{1}H-NMR measurement (solvent: D_2O; temperature: 25 °C). The compositions of PEG-*b*-P(Glu) are abbreviated as PEG-*b*-P(Glu) 12–20, PEG-*b*-P(Glu) 12–40 and PEG-*b*-P(Glu) 12–70 for the different P(Glu) block lengths (20, 40, and 70 U, respectively).

2.4. Preparation of DACHPt-loaded micelles (DACHPt/m)

DACHPt/m were prepared according to a previously described method [22]. Briefly, DACHPt (5 mM) was suspended in distilled water and mixed with silver nitrate ([$AgNO_3$]/[DACHPt]=1) to form an aqueous complex. The solution was kept in the dark at 25 °C for 24 h. AgCl precipitates found after the reaction were eliminated by centrifugation. Afterward, the supernatant was purified by passage through a 0.22 μm filter. Then, PEG-*b*-P(Glu) 12–20, 12–40, or 12–70 ([Glu]=5 mmol/liter) was added to DACHPt aqueous complex solution ([DACHPt]/[Glu]=1.0) and reacted for 120 h to prepare DACHPt/m. The prepared micelles were purified by ultrafiltration [molecular weight cutoff size (MWCO): 100,000]. The size distribution of DACHPt/m was evaluated by the dynamic light scattering (DLS) measurement at 25 °C using a Photal DLS-7000 dynamic laser scattering spectrometer (Otsuka Electronics, Osaka, Japan). The zeta-potential of DACHPt/m was determined using a Zetasizer Nano ZS90 (Malvern Instruments, Worcestershire, United Kingdom). The Pt content of the micelles was determined by an ion coupled plasma-mass spectrometer (4500 ICP-MS; Hewlett Packard, Palo Alto, CA).

2.5. Biodistribution

In order to analyze the fate of oxaliplatin and DACHPt/m *in vivo*, CDF_1 mice (female, n=6) were injected subcutaneously with C-26 cells (1×10^6 cells/ml). Fourteen days later, oxaliplatin or DACHPt/m prepared with PEG-*b*-P(Glu) 12–40 were intravenously injected by the tail vein at a dose of 100 μg/mouse on a platinum basis. Mice were sacrificed after defined time periods (1, 4, 8, 24, 48, and 72 h).

To assess the effect of formulation on the tissue distribution, CDF_1 mice (female, n=6) bearing s.c. C-26 tumors were intravenously administered oxaliplatin or DACHPt/m prepared with PEG-*b*-P(Glu) with different P(Glu) lengths (20, 40, and

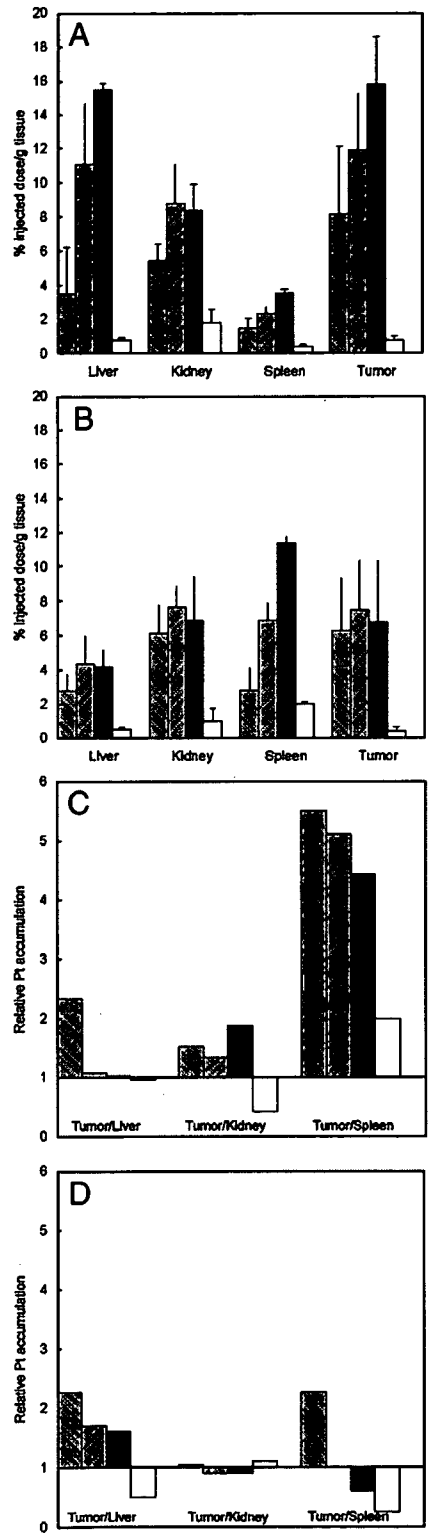

Fig. 3. Biodistribution of DACHPt-loaded micelle (DACHPt/m) prepared with PEG-*b*-P(Glu) 12–20(▨), PEG-*b*-P(Glu) 12–40(▨), PEG-*b*-P(Glu) 12–70(■) and oxaliplatin (□): A. 24 h; B.48 h; C. 24 h tumor/organ ratio; D. 48 h tumor/organ ratio. Data are expressed as averages±S.D.

70 U) at 100 μg/mouse on a platinum basis. Mice were sacrificed at 24 and 48 h post-incubation.

Tumor, liver, kidney, spleen, and muscle were collected. Blood was collected from the inferior vena cava, heparinized and centrifuged to obtain the plasma. Tissue samples were washed in ice-cold saline and weighed after removing excess fluid. All samples were dissolved in HNO_3 and evaporated to dryness. The Pt concentration was measured by ICP-MS after the samples were redissolved in 5 N HCl. The area under the curve (AUC) was calculated by the trapezoidal rule.

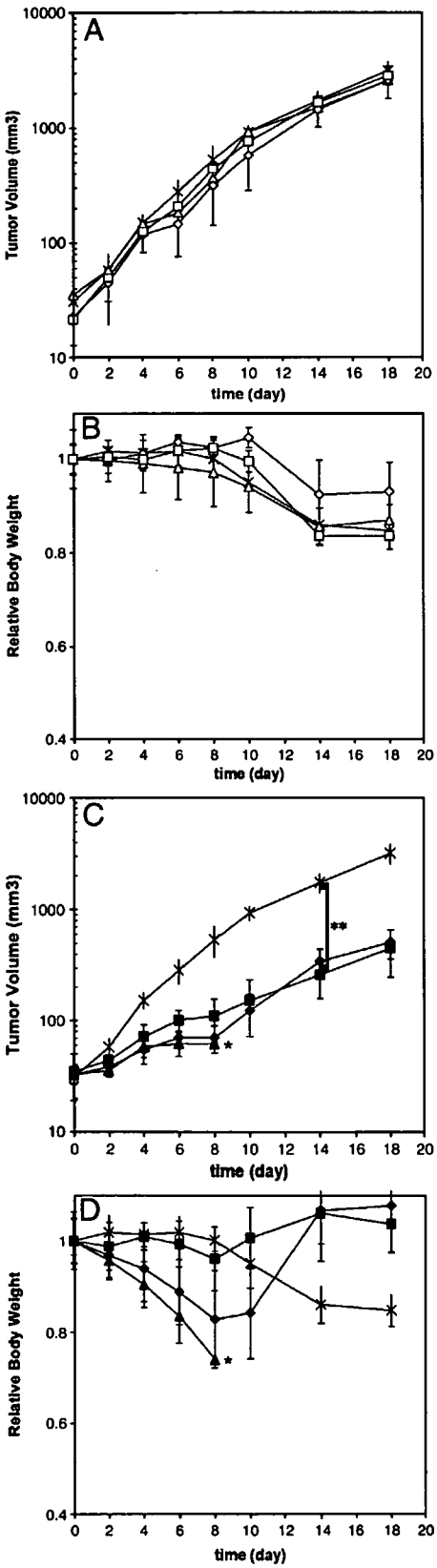

Fig. 4. Antitumor activity of DACHPt-loaded micelle (DACHPt/m) prepared with PEG-*b*-P(Glu) 12–40 against s.c. C-26 tumor model ($n=5$). Saline(×); oxaliplatin at 6 mg/kg(△); 4 mg/kg(◇); 2 mg/kg(□). DACHPt-loaded micelle (DACHPt/m) 12–40 at 6 mg/kg(▲); 4 mg/kg(◆); 2 mg/kg(■). A. Tumor volume (mm^3) for oxaliplatin treatment; B. Relative body weight of mice for oxaliplatin treatment; C. Tumor volume (mm^3) for DACHPt/m treatment; D. Relative body weight of mice for DACHPt/m treatment. Data are expressed as averages±S.D. *Toxic death. **$p<0.001$.

2.6. Antitumor activity assay

CDF_1 mice (female, $n=6$) were inoculated subcutaneously with C-26 cells (1×10^6 cells/ml). Tumors were allowed to grow for 1 week (the size of tumor at this point was approximately 30 mm^3 or 100 mm^3). Subsequently, mice were treated i.v. 4 times at 2-day intervals at doses of 2, 4, 6 and 10 mg/kg of oxaliplatin or 2, 4 and 6 mg/kg (on a platinum base) of DACHPt/m prepared with PEG-*b*-P(Glu) 12–20 or PEG-*b*-P (Glu) 12–40. The antitumor activity was evaluated in terms of tumor size (V), as estimated by the following equation:

$$V = a \times b^2/2$$

where a and b are the major and minor axes of the tumor measured by a caliper, respectively. The body weight was measured simultaneously and was taken as a parameter of systemic toxicity. The statistical analysis of animal data was carried out by the unpaired t-test.

2.7. Antitumor activity in a bioluminescent intraperitoneal metastasis model

SCID mice (female, $n=5$) were inoculated intraperitoneally with Hela-Luc cells (5×10^5 cells/ml). Tumors were allowed to grow for 3 days. Subsequently, mice were treated i.v. 3 times at 2-day intervals at doses of 4 and 6 mg/kg (on a platinum base) of oxaliplatin or DACHPt/m prepared with PEG-b-P(Glu) 12–20. *In vivo* bioluminescent imaging (BLI) was performed with an IVIS Imaging System (Xenogen) comprised of a highly sensitive, cooled CCD camera mounted in a light-tight specimen box. Images and measurements of bioluminescent signals were acquired and analyzed using Living Image software (Xenogen). Ten minutes prior to *in vivo* imaging, animals received the substrate D-luciferin (Biosynth) at 150 mg/kg in PBS by intraperitoneal injection and were anesthetized using 1–3% isoflurane (Abbott Laboratories, North Chicago, IL). Animals were placed onto a warmed stage inside the camera box and received continuous exposure to 1–2% isoflurane to sustain sedation during imaging. Imaging times ranged from 10 to 60 s, depending on the bioluminescence of the metastatic lesions. Five mice were imaged at a time. Tumor growth was monitored

by BLI every second day for 18 days. The light emitted from the bioluminescent tumors was detected *in vivo* by the IVIS Imaging System, was digitized and electronically displayed as a pseudocolor overlay onto a gray scale animal image. Regions of interest (ROI) from displayed images were drawn around the tumor sites and quantified as photons/second using the Living Image software. The statistical analysis of animal data was carried out by the unpaired *t*-test.

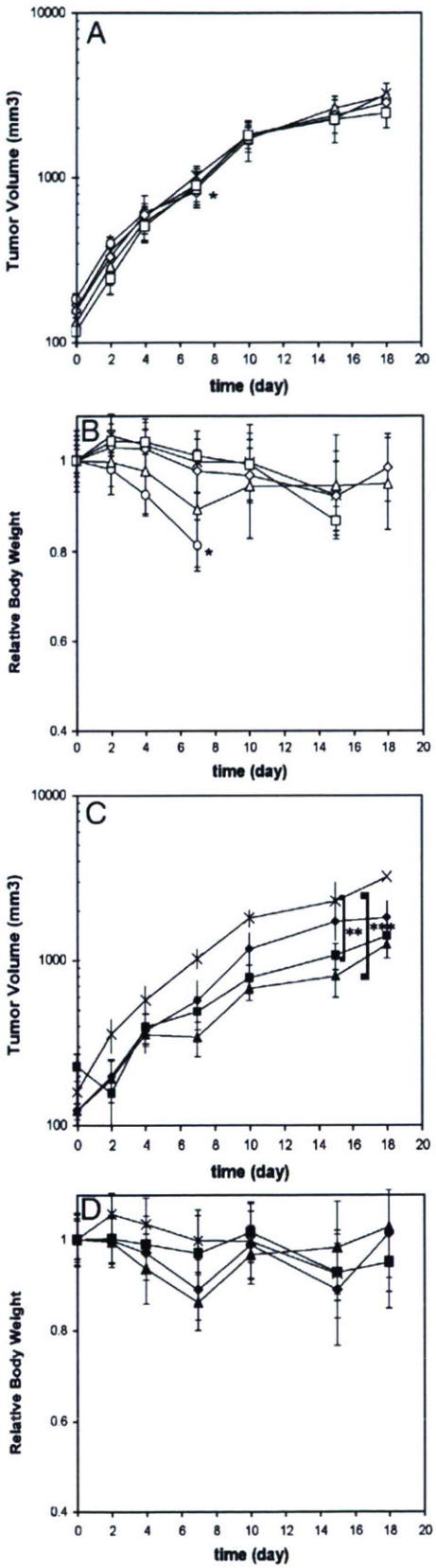

Fig. 5. Antitumor activity of DACHPt-loaded micelle (DACHPt/m) prepared with PEG-*b*-P(Glu) 12–20 against s.c. C-26 tumor model ($n=6$). Saline(×); oxaliplatin at 10 mg/kg(○); 6 mg/kg(△); 4 mg/kg(◇); 2 mg/kg(□). DACHPt-loaded micelle (DACHPt/m) 12–20 at 6 mg/kg(▲); 4 mg/kg(◆); 2 mg/kg(■). A. Tumor volume (mm^3) for oxaliplatin treatment; B. Relative body weight of mice for oxaliplatin treatment; C. Tumor volume (mm^3) for DACHPt/m treatment; D. Relative body weight of mice for DACHPt/m treatment. Data are expressed as averages±S.D. *Toxic death. **$p<0.01$. ***$p<0.005$.

3. Results

3.1. Micelle characterization

The metal-polymer complex formation between DACHPt and the carboxylic group of the p(Glu) in the PEG-*b*-P(Glu) led to the formation of narrowly distributed micellar assemblies (Fig. 1) with average diameters of approximately 40 nm (Table 1). The increase in the length of the p(Glu) block slightly enlarged the diameter of DACHPt/m (Table 1). The drug content in the micelles was determined to be remarkably high in all the micelle formulations (Table 1). The [DACHPt]/[Glu] molar ratios in DACHPt/m were found to be similar for all the formulations.

3.2. Biodistribution

3.2.1. Biodistribution of free oxaliplatin and DACHPt/m prepared with PEG-b-P(Glu) 12–40

The biodistribution study was performed on CDF_1 mice ($n=6$) bearing s.c. C-26 tumors. Oxaliplatin or DACHPt/m prepared with PEG-*b*-P(Glu) 12–40 were i.v. injected. In previous studies, DACHPt/m prepared with PEG-*b*-P(Glu) 12–40 have shown remarkably prolonged blood circulation, whereas free oxaliplatin was promptly removed from circulation. The Pt in plasma was determined to be 15% of the injected dose at 24 h post-injection, and more than 8% even at 48 h after injection for DACHPt/m [22]. This prolonged blood circulation of DACHPt/m was reasonably associated with the high kinetic stability of the micelles in phosphate buffered saline at 37 °C [22].

The accumulations of oxaliplatin and DACHPt/m in normal tissues (kidney, liver, spleen, and muscle) and solid tumor (C-26 cells) are shown in Fig. 2. Oxaliplatin was rapidly distributed to each organ in agreement with its rapid plasma clearance. In contrast, DACHPt/m showed cumulative accumulation in each organ and solid tumor ($p<0.001$) due to its remarkably prolonged blood circulation time, and the Pt level in the liver, spleen, and tumor continuously increased up to approximately 48 h after injection (Fig. 2). Consequently, the DACHPt/m exhibited 20-, 4-, and 25-fold higher accumulation in the liver, spleen, and tumor, respectively, than oxaliplatin at 48 h after injection. To assess the selectivity to the solid tumor, the

accumulation ratios and area under the Pt concentration-time curve (AUC) ratios of the tumor to normal tissues at 48 h after injection are summarized in Table 2. The area under the Pt concentration-time curve was calculated based on the trapezoidal rule up to 48 h. As shown in Table 2, the tumor to kidney, liver and spleen ratios were lower than 1 for oxaliplatin, suggesting no selectivity to the tumor. In contrast, the DACHPt/m exhibited accumulation and AUC ratios higher than 1.0, suggesting its selective accumulation in the tumor.

3.2.2. *Effect of P(Glu) block length on the biodistribution of micelles*

The biodistribution of the micelles prepared from PEG-*b*-P(Glu) with different p(Glu) block units in tumor-bearing mice was examined and is shown in Fig. 3. The Pt accumulation levels were studied at 24 and 48 h. All the DACHPt/m formulations showed elevated Pt levels at the tumor (Fig. 3A and B). Importantly, the amount of Pt in liver was directly correlated with the length of the p(Glu) block forming DACHPt/m. The tumor targeting efficiency of the micelles was estimated by calculating the ratio of the accumulated dose in the tumor site against the accumulated dose in the organs (Fig. 3C and D). From these results, DACHPt delivery to the tumor site by a micellar carrier seems to be extremely efficient, since all the micelles showed higher tumor/organ accumulation ratios. This efficiency was maximized for the PEG-*b*-P(Glu) 12–20-micelle formulation showing the lowest non-specific accumulation in normal tissues, thus achieving the highest relative tumor targeting. Such enhanced tumor targeting will permit expanding the therapeutic window of the micelle.

3.3. *Antitumor activity*

To evaluate the antitumor activity of DACHPt/m, CDF1 mice ($n=6$) bearing subcutaneous C-26 cells were treated i.v. four times at 2-day intervals with oxaliplatin at doses of 2, 4, 6, and 10 mg/kg or DACHPt/m (prepared with PEG-*b*-P(Glu) 12–40 and 12–20) at doses of 2, 4, and 6 mg/kg on a Pt basis. Each drug was intravenously injected on days 7, 9, 11, and 13 after inoculation, and the tumor volume after the treatment by oxaliplatin or DACHPt/m with PEG-*b*-P(Glu) 12–40 and 12–20 is shown in Figs. 4 and 5 (A and C), respectively. The relative body weight after the treatment was also monitored and shown in Figs. 4 and 5 (B and D).

The mice treated with 10 mg/kg of oxaliplatin showed toxic death after the fourth injection. Although animals treated with lower oxaliplatin doses did not show significant body weight loss, no inhibition of the tumor growth rate was observed ($p>0.05$). In contrast, the mice treated with 2 mg/kg of DACHPt/m prepared with PEG-*b*-P(Glu) 12–40 achieved significant reduction in the tumor growth rate ($p<0.001$ at day 14) without showing any body weight loss (Fig. 4C and D). Even higher tumor growth inhibition was observed for the mice treated with 4 mg/kg of PEG-*b*-P(Glu) 12–40 DACHPt/m

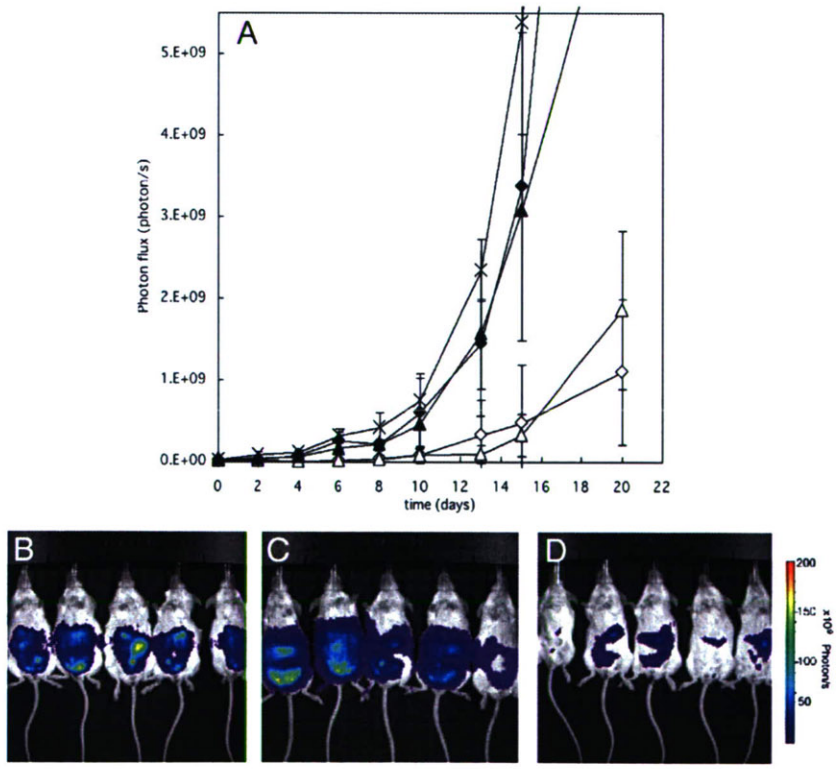

Fig. 6. Antitumor activity of DACHPt-loaded micelle (DACHPt/m) prepared with PEG-*b*-P(Glu) 12–20 against i.p. HeLa-Luc metastases ($n=5$). A. Relative photon flux from intraperitoneal metastatic sites of HeLa-luc *in vivo* treated with oxaliplatin or DACHPt-loaded micelle (DACHPt/m): Saline(×); oxaliplatin at 6 mg/kg(▲); 4 mg/kg(◆); DACHPt/m 12–20 at 6 mg/kg(△); 4 mg/kg(◇). Data are expressed as averages±S.D. *In vivo* bioluminescent images from HeLa-Luc i.p metastases at day 15: B. Saline; C. oxaliplatin 6 mg/kg; D. DACHPt/m 12–20 at 6 mg/kg.

($p<0.001$ at day 14); however, the 20% body weight loss after fourth injection suggests toxicity intensification. Increasing the DACHPt/m dose to 6 mg/kg resulted in 4 toxic deaths at day 8. The PEG-*b*-P(Glu) 12–20 micelle formulation reduced the toxicity while retaining the antitumor activity of the micelle (Fig. 5C and D). At 2 mg/kg or 4 mg/kg, this micelle formulation showed improved antitumor effect ($p<0.05$ at day 15 for 2 mg/kg; $p<0.01$ at day 15 for 4 mg/kg) compared with oxaliplatin without showing any body weight loss. At 6 mg/kg, the best tumor growth rate reduction was achieved ($p<0.005$ at day 15). The highest dose of this formulation in this experiment did not reach the lethal dose. Thus, PEG-*b*-P(Glu) 12–20 formulation for DACHPt/m seems to radically reduce drug toxicity with maintaining its potent antitumor effect, thus enlarging the therapeutic window. In addition, toxic death with DACHPt/m appeared at lower drug equivalent concentration than with oxaliplatin mainly due to the extremely high plasma AUC of DACHPt/m [22], but also because oxaliplatin is a prodrug of DACHPt. Thus, even though the drug equivalent of DACHPt/m to induce toxic death should be compared with DACHPt, it is very difficult to administer DACHPt alone due to its poor solubility.

Since DACHPt/m prepared with PEG-P(Glu) 12–70 showed higher accumulation to the liver and spleen than DACHPt/m prepared from PEG-P(Glu) 12–20 and 12–40, it will probably not increase the efficiency of the carrier. Therefore, its antitumor activity was not tested.

3.4. Antitumor activity in a bioluminescent intraperitoneal metastasis model

To evaluate the *in vivo* antitumor effect of DACHPt/m on multiple metastases generated from i.p inoculated Hela-Luc cells, SCID mice ($n=5$) were treated with free oxaliplatin or DACHPt/m beginning on day 4 post-injection. Mice with images indicating a successful i.p. inoculation on day 0 and showing *in vivo* evidence of metastasis by day 4 were placed in the drug treatment group. Free oxaliplatin or DACHPt/m were administered i.v a total of three times on day 0, 2, and 4. To quantify the bioluminescent data from metastasis, the photons emitted from the ROI in the whole animal (ventral images) were measured. The mean total photons/s were calculated from all mice. The *in vivo* bioluminescent data indicated that there was a 10-to 50-fold drop in the signal after DACHPt/m treatment (Fig. 6A). Images taken on day 15 (Fig. 6B, C, and D) indicated that DACHPt/m reduced tumor spreading in the peritoneal cavity, showing their strong growth inhibitory effect against the metastatic tumors.

4. Discussion

DACHPt/m were designed to have an extended blood circulation and a selective and high accumulation at the tumor site by the EPR effect. The average diameter of 40 nm and the hydrophilic PEG shell surrounding the micelle core are determinant features of DACHPt/m to avoid the uptake by the RES. Moreover, the sub-100 nm size of micellar nanocarriers might be optimal to achieve a remarkably high tumor extravasation efficiency and deep tumor penetration regardless of the tumor type [26]. The pharmacokinetic parameters of polymeric micelles are significantly modulated by the copolymer architecture. In this regard, the length of the micelle core-forming block not only determines the drug loading capacity of the micelle but also contributes largely to the physicochemical properties of the micelles, whereas PEG length and PEG surface density of micelles have been strongly associated with their long-circulating properties [27,28]. In this study, we prepared DACHPt/m using PEG-*b*-P(Glu) bearing different lengths of p (Glu) chain. We found that this variation considerably influences the biodistribution of micelles and thereby their antitumor activity as well as the final therapeutic window.

Drug dosage in chemotherapy is decided in part based on the competing goals of maximizing the death of malignant cells while minimizing damage to healthy cells. In the case of oxaliplatin, the major and most frequent dose-limiting toxicity observed in clinical trials was neurotoxicity [1]. Toxicological studies performed on rats with cisplatin and oxaliplatin demonstrated that the main target of neurotoxicity was the dorsal root ganglion (DRG) [29]. Although cisplatin accumulated in the DRG at a higher extent than oxaliplatin, the latter displayed more morphometric changes to the DRG after an 8-week recovery period, and this was correlated with a greater retention of oxaliplatin by the DRG in comparison with cisplatin. In contrast, neurotoxic studies revealed that CDDP-loaded micelles did not show any neurotoxicity or neuronal degeneration in rats [21]. This result might be attributed to the marked restriction of platinum accumulation into nervous tissue for the CDDP-loaded micelle, owing to the micelle size and its hydrophilic surface. Since CDDP-loaded micelles and DACHPt/m showed comparable prolonged blood circulation, preferential tumor targeting, and low accumulation in organs (Fig. 2) [20], similar reduction in the platinum accumulation at nervous tissue should be expected for DACHPt/m. Moreover, it has also been suggested that the oxalate group on oxaliplatin might immobilize calcium ions, thereby altering the amplitude of voltage-gated sodium channels of neurons [30]. The absence of an oxalate group in the DACHPt/m formulations eliminates this kind of neuronal damage.

The use of oxaliplatin is also associated with the development of severe sinusoidal injury, an aspect that had not been considered in the earlier clinical trials of oxaliplatin [31,32]. In this regard, the CDDP-loaded micelle prepared with PEG-*b*-P(Glu) 12–40 has shown transient hepatic dysfunction in rats directly related to accumulation of the micelle in liver [21]. In the present study, DACHPt/m prepared with PEG-*b*-P(Glu) 12–40 showed biphasic behavior in liver accumulation, and the Pt level in the liver remarkably increased after 8 h post-injection (Fig. 2B). Thus, the avoidance of liver uptake would be critical for the development of a clinically effective DACHPt/m formulation. We previously reported that the CDDP-loaded micelles also showed rapid accumulation of the micelle in the liver due to the morphological changes of the micelle accompanied by the release of CDDP during circulation [20]. However, such liver accumulation of the CDDP-loaded micelles was reduced for the micelle formulation from PEG-*b*-P(Glu) with a longer PEG segment [20]. Thus, the

coverage of the nanoparticles with PEG palisades is likely to be a crucial factor in the reduced liver accumulation. In this study, we evaluated the effects of the P(Glu) lengths of PEG-*b*-P(Glu) on the accumulation of the micelles in normal tissues and tumors. As a result, the micelles prepared with PEG-*b*-P(Glu) 12–20 showed considerably reduced accumulation in the liver (Fig. 3), resulting in critically reduced toxicity and, in particular, permitted a dosage increase (Fig. 5). Possibly, the use of PEG-*b*-P(Glu) with shorter P(Glu) segments may allow the formation of DACHPt/m with effective surface coverage by PEG probably due to reduced micellar core size, leading to reduction of the liver accumulation of the micelles.

DACHPt/m, prepared with PEG-b-P(Glu) 12–40 or 12–20, presented a remarkable, statistically relevant *in vivo* antitumor activity (Figs. 4 and 5), whereas free oxaliplatin failed to suppress tumor growth. The improved performance of DACHPt/m could be attributed to several aspects. The most distinguishable one is the high and preferential accumulation of DACHPt/m in the tumor due to the prolonged circulation of micelles in the bloodstream as well as the aforementioned EPR effect. In this study, DACHPt/m showed 10 times higher tumor accumulation than free oxaliplatin after 24-h post-injection, and such accumulation was maintained for an extended period (Figs. 2 and 3). On the other hand, free oxaliplatin was rapidly cleared from the bloodstream and the drug level at the tumor site was particularly low (Fig. 2). This accumulation level may be lower than the minimal amount needed to attain an efficient *in vivo* antitumor activity.

The avoidance of permanent drug inactivation by protein binding through the complexation of the platinum to the carboxylic groups in the micelle core could also be responsible for the improved biological performance of DACHPt/m over oxaliplatin. It was previously reported that, immediately after a 1 h infusion of oxaliplatin, approximately 5–30% of the drug is unbound, 10–30% is protein-bound, and 40% form complexes with hemoglobin and small molecular weight compounds in erythrocytes. Three hours later, no oxaliplatin is detectable in the plasma ultrafiltrate and only 10% is detectable in urine [33,34]. Furthermore, as many as 17 biotransformation products of oxaliplatin have been described (conjugation with methionine, cysteine, glutathione, and other low molecular weight species), but only the minor complexes $DACHPtCl_2$, $[DACHPt(H_2O)Cl]^+$ and $[DACHPt(H_2O)_2]^{2+}$ retain the ability to bind to DNA to exert the cytotoxic activity [35,36]. Among them, the dihydroxy product of oxaliplatin has been shown to have significantly greater cellular uptake and cytotoxic properties than its parent compound [37]. However, it represents a very small amount of the total plasma platinum pool after oxaliplatin administration, and therefore might not be a determinant for oxaliplatin cytotoxicity. Moreover, the formation process of $[DACHPt(H_2O)_2]^{2+}$ involves the formation of a reversible intermediate, oxalato monodentate compound, and the dissociation constant for the ring-opening step is below physiological pH (pKa=7.16). This implies that at physiological pH, the reaction favors the deprotonation of the open-ring form and the subsequent formation of the dihydroxy complex, whereas under the acidic conditions of solid tumors, ring-closure is favored and the rapid formation of oxaliplatin would be expected [38]. For DACHPt/m, the biotransformation products might be considerably different from those of oxaliplatin, and probably affect the *in vivo* performance of the drug. Since the discharge of DACHPt products from the micelle core occurs only after cleavage of the polymer-metal complex by chloride ions, and this release is enhanced at low pH, DACHPt/m probably set up conditions that favor the formation of active complexes of oxaliplatin, including the highly active $[DACHPt(H_2O)_2]^{2+}$, leading to an improved efficacy of the drug. Moreover, selective intracellular release of DACHPt complexes might occur after internalization of the micelles by endocytosis in cancer cells. As a result, DACHPt complexes may avoid extracellular inactivation and may readily induced intracellular damage.

Since systemic chemotherapy is not regarded as curative in patients with metastatic tumors and all the established therapies show low efficiency at the late stage of the disease, the antitumor activity of DACHPt/m against an i.p. metastatic tumor model was evaluated to test the potential use of micelles as a therapeutic strategy. Monitoring the development of metastatic disease is currently possible *in vivo* with the use of small animal imaging technologies including bioluminescent imaging. The results demonstrate that free oxaliplatin failed to suppress HeLa-Luc metastatic growth at any dose, whereas DACHPt/m showed a high antitumor activity while controlling tumor dissemination in the peritoneal cavity. This marked difference could be correlated to the extended blood circulation and preferential tumor accumulation of DACHPt/m, although further experiments are necessary to determine the effect of the metastatic disposition on the efficiency of the micelle. The present results revealed that DACHPt/m has a high level of antitumor activity not only on primary solid tumors but also against metastatic tumors, suggesting that DACHPt/m could be an outstanding drug delivery system for metastasis treatment.

In conclusion, we have demonstrated that decreasing the length of the core-forming block of DACHPt/m augmented their tumor specificity and drastically diminished their toxicity. Moreover, the high and preferential accumulation of the micelles at the tumor site resulted in considerable antitumor activity of DACHPt/m against primary and metastatic tumor models. Thus, DACHPt/m might be an exceptional drug delivery system for oxaliplatin active complexes.

Acknowledgments

This research was supported by a Grant-in-Aid for Scientific Research from Ministry of Education, Culture, Sports, Science and Technology of Japan as well as by the Project on the Materials Development for Innovative Nano-Drug Delivery Systems from the Ministry of Education, Culture, Sports, Science and Technology (MEXT), Japan.

References

[1] A. Ibrahim, S. Hirschfeld, M.H. Cohen, D.J. Griebel, G.A. Williams, R. Pazdur, FDA drug approval summaries: oxaliplatin, Oncologist 9 (2004) 8–12.

[2] J.M. Extra, M. Espie, F. Calvo, Phase I study of oxaliplatin in patients with advanced cancer, Cancer Chemother. Pharmacol. 25 (1990) 299–303.

[3] G. Mathé, Y. Kidani, M. Segiguchi, M. Eriguchi, G. Fredj, G. Peytavin, J.L. Misset, S. Brienza, F. de Vassals, E. Chenu, C. Bourut, Oxalato-platinum or l-OHP, a third generation platinum complex: an experimental and clinical appraisal and preliminary comparison with cis-platinum and carboplatinum, Biomed. Pharmacother. 43 (1989) 237–250.
[4] Y. Matsumura, H. Maeda, A new concept for macromolecular therapeutics in cancer chemotherapy: mechanism of tumoritropic accumulation of proteins and the antitumor agent SMANCS, Cancer Res. 46 (1986) 6387–6392.
[5] M. Yatvin, H. Miihlensiepen, W. Porschen, L. Feinendegen, J. Weinstein, Selective delivery of liposome-associated cis-dichloro-diammine platinum (II) by heat and its influence on tumor drug uptake and growth, Cancer Res. 41 (1981) 1602–1607.
[6] R. Perez-Soler, Liposomes as carriers of antitumor agents: toward a clinical reality, Cancer Treatment Rev. 16 (1989) 67–82.
[7] R. Perez-Soler, I. Han, S. Al-Baker, A.R. Khokhar, Lipophilic platinum complexes entrapped in liposomes: improved stability and preserved antitumor activity with complexes containing linear alkyl carboxylate leaving groups, Cancer Chemother. 33 (1994) 378–384.
[8] D. Avichechter, B. Schechter, R. Arnon, Functional polymers in drug delivery: carrier-supported CDDP (cis-platin) complexes carboxylates — effect on human ovarian carcinoma, React. Funct. Polym. 36 (1998) 59–69.
[9] B. Schechner, A. Newman, M. Wilnek, R. Arnon, Soluble polymers as carriers of cis-platinum, J. Control. Release 39 (1989) 75–87.
[10] X. Lin, Q. Zhang, J.R. Rice, D.R. Stewart, D.P. Nowotnik, S.B. Howell, Improved targeting of platinum chemotherapeutics. The antitumour activity of the HPMA copolymer platinum agent AP5280 in murine tumour models, Eur J Cancer. 40 (2004) 291–297.
[11] J.R. Rice, J.L. Gerberich, D. Nowotnik, S.B. Howell, Preclinical efficacy of AP5346, a novel diaminocyclohexane-platinum tumor-targeting drug delivery system, Clin. Cancer Res. 12 (2006) 2248–2254.
[12] K. Kataoka, G.S. Kwon, M. Yokoyama, Y. Sakurai, T. Okano, Block copolymer micelles as vehicles for drug delivery, J. Control. Release 24 (1993) 119–132.
[13] C. Allen, D. Mysinger, A. Eisenberg, Nano-engineering block copolymer aggregates for drug delivery, Colloids Surf., B Biointerfaces 16 (1999) 3–27.
[14] N. Nishiyama, K. Kataoka, Nano-structured devices based on block copolymer assemblies for drug delivery: designing structures for enhanced drug function, Adv. Polym. Sci. 193 (2006) 67–101.
[15] H.M. Aliabadi, A. Lavasanifar, Polymeric micelles for drug delivery, Expert Opin. Drug Deliv. 3 (2006) 139–161.
[16] N. Nishiyama, M. Yokoyama, T. Aoyagi, T. Okano, Y. Sakurai, K. Kataoka, Preparation and characterization of self-assembled polymer-metal complex micelle from cis-dichlorodiammineplatinum(II) and poly(ethylene glycol)-poly(a,b-aspartic acid) block copolymer in an aqueous medium, Langmuir 15 (1999) 377–383.
[17] N. Nishiyama, K. Kataoka, Preparation and characterization of size-controlled polymeric micelle containing cis-dichlorodiammineplatinum(II) in the core, J Control. Release 74 (2001) 83–94.
[18] N. Nishiyama, Y. Kato, Y. Sugiyama, K. Kataoka, Cisplatin-loaded polymer-metal complex micelle with time-modulated decaying property as a novel drug delivery system, Pharm. Res. 18 (2001) 1035–1041.
[19] N. Nishiyama, F. Koizumi, S. Okazaki, Y. Matsumura, K. Nishio, K. Kataoka, Differential gene expression profile between PC-14 cells treated with free cisplatin and cisplatin-incorporated polymeric micelles, Bioconjug. Chem. 14 (2003) 449–457.
[20] N. Nishiyama, S. Okazaki, H. Cabral, M. Miyamoto, Y. Kato, Y. Sugiyama, K. Nishio, Y. Matsumura, K. Kataoka, Novel cisplatin-incorporated polymeric micelles can eradicate solid tumors in mice, Cancer Res. 63 (2003) 8977–8983.
[21] H. Uchino, Y. Matsumura, T. Negishi, F. Koizumi, T. Hayashi, T. Honda, N. Nishiyama, K. Kataoka, S. Naito, T. Kakizoe, Cisplatin-incorporating polymeric micelles (NC-6004) can reduce nephrotoxicity and neurotoxicity of cisplatin in rats, Br. J. Cancer 93 (2005) 678–687.
[22] H. Cabral, N. Nishiyama, S. Okazaki, H. Koyama, K. Kataoka, Preparation and biological properties of dichloro(1,2-diaminocyclohexane)platinum (II) (DACHPt)-loaded polymeric micelles, J. Control. Release 101 (2005) 223–232.
[23] T. Tashiro, Y. Kawada, Y. Sakurai, Y. Kidani, Antitumor activity of a new platinum complex: oxalato (trans-l-diaminocyclohexane) platinum (II): new experimental data, Biomed. Pharmacother. 43 (1989) 251–260.
[24] S. Oppenheimer, Cellular basis of cancer metastasis: a review of fundamentals and new advances, Acta Histochem. 108 (2006) 327–334.
[25] Cervical cancer, NIH Consens. Statement 14 (1996) 1–38.
[26] A. Lukyanov, Z. Gao, L. Mazzola, V.P. Torchilin, Polyethylene glycol-dyacyllipid micelles demonstrate increased accumulation in subcutaneous tumors in mice, Pharm. Res. 19 (2002) 1424–1429.
[27] G.S. Kwon, S. Suwa, M. Yokoyama, T. Okano, Y. Sakurai, K. Kataoka, Enhanced tumor accumulation and prolonged circulation times of micelles-forming poly(ethyleneoxide-aspartate) block copolymers-adriamycin conjugates, J. Control. Release 29 (1994) 17–23.
[28] M. Yokoyama, T. Okano, Y. Sakurai, S. Fukushima, K. Okamoto, K. Kataoka, Selective delivery of adriamycin to a solid tumor using a polymeric micelle carrier system, J. Drug Target. 7 (1999) 171–186.
[29] G. Cavaletti, G. Tredici, M.G. Petruccioli, E. Donde, P. Tredici, P. Marmiroli, C. Minoia, A. Ronchi, M. Bayssas, G. Griffon Etienne, Effects of different schedules of oxaliplatin treatment on the peripheral nervous system of the rat, Eur. J. Cancer 37 (2001) 2457–2463.
[30] F. Grolleau, L. Gamelin, M. Boisdron-Celle, B. Lapied, M. Pelhate, E. Gamelin, A possible explanation for a neurotoxic effect of the anticancer agent oxaliplatin on neuronal voltage-gated sodium channels, J. Neurophysiol. 85 (2001) 2293–2297.
[31] L. Rubbia-Brandt, V. Audard, P. Sartoretti, A.D. Roth, C. Brezault, M. Le Charpentier, B. Dousset, P. Morel, O. Soubrane, S. Chaussade, G. Mentha, B. Terris, Severe hepatic sinusoidal obstruction associated with oxaliplatin based chemotherapy in patients with metastatic colorectal cancer, Ann. Oncol. 15 (2004) 460–466.
[32] G. Tisman, D. MacDonald, N. Shindell, E. Reece, P. Patel, N. Honda, E.K. Nishimora, J. Garris, W. Shannahan, N. Chisti, J. McCarthy, S.N. Moaddeli, D. Sargent, A. Plant, Oxaliplatin toxicity masquerading as recurrent colon cancer, J. Clin. Oncol. 22 (2004) 3202–3204.
[33] J. Liu, E. Kraut, J. Bender, R. Brooks, S. Balcerzak, M. Grever, H. Stanley, S. D'Ambrosio, R. Gibson-D'Ambrosio, K.K. Chan, Pharmacokinetics of oxaliplatin (NSC266046) alone and in combination with paclitaxel in cancer patients, Cancer Chemother. Pharmacol. 49 (2002) 367–374.
[34] C. Massari, S. Brienza, M. Rotarski, J. Gastiaburu, J.-L. Misset, D. Cupissol, E. Alafaci, H. Dutertre-Catella, G. Bastian, Pharmacokinetics of oxaliplatin in patients with normal versus impaired renal function, Cancer Chemother. Pharmacol. 45 (2000) 157–164.
[35] F.R. Luo, S.D. Wyrick, S.G. Chaney, Biotransformations of oxaliplatin in rat blood *in vitro*, J. Biochem. Molec. Toxicol. 13 (1999) 159–169.
[36] F.R. Luo, T.-Y. Yen, S.D. Wyrick, S.G. Chaney, High-performance liquid chromatographic separation of the biotransformation products of oxaliplatin, J. Chromatogr., B 724 (1999) 345–356.
[37] F.R. Luo, S.D. Wyrick, S.G. Chaney, Cytotoxicity, cellular uptake and cellular biotransformations of oxaliplatin in human colon carcinoma cells, Oncol. Res. 10 (1998) 595–603.
[38] E. Jerremalm, P. Videhult, G. Alvelius, W.J. Griffiths, T. Bergman, S. Eksborg, H. Ehrsson, Alkaline hydrolysis of oxaliplatin — isolation and identification of the oxalato monodentate intermediate, J. Pharm. Sci. 91 (2002) 2116–2121.